The Astrophysical Journal, 767:6 (9pp), 2013 April 10 doi:10.1088/0004-637X/767/1/6

ACCELERATION OF LOW-ENERGY IONS AT PARALLEL SHOCKS WITH A FOCUSED TRANSPORT MODEL

Pingbing Zuo, Ming Zhang, and Hamid K. Rassoul
Department of Physics and Space Sciences, Florida Institute of Technology, Melbourne, FL 32901, USA
Received 2012 November 14; accepted 2013 February 9; published 2013 March 19

ABSTRACT

We present a test particle simulation on the injection and acceleration of low-energy suprathermal particles by parallel shocks with a focused transport model. The focused transport equation contains all necessary physics of shock acceleration, but avoids the limitation of diffusive shock acceleration (DSA) that requires a small pitch angle anisotropy. This simulation verifies that the particles with speeds of a fraction of to a few times the shock speed can indeed be directly injected and accelerated into the DSA regime by parallel shocks. At higher energies starting from a few times the shock speed, the energy spectrum of accelerated particles is a power law with the same spectral index as the solution of standard DSA theory, although the particles are highly anisotropic in the upstream region. The intensity, however, is different from that predicted by DSA theory, indicating a different level of injection efficiency. It is found that the shock strength, the injection speed, and the intensity of an electric cross-shock potential (CSP) jump can affect the injection efficiency of the low-energy particles. A stronger shock has a higher injection efficiency. In addition, if the speed of injected particles is above a few times the shock speed, the produced power-law spectrum is consistent with the prediction of standard DSA theory in both its intensity and spectrum index with an injection efficiency of 1. CSP can increase the injection efficiency through direct particle reflection back upstream, but it has little effect on the energetic particle acceleration once the speed of injected particles is beyond a few times the shock speed. This test particle simulation proves that the focused transport theory is an extension of DSA theory with the capability of predicting the efficiency of particle injection.

Key words: acceleration of particles – diffusion – methods: numerical – shock waves

Online-only material: color figures

1. INTRODUCTION

The most commonly accepted theory for particle acceleration at shock waves is diffusive shock acceleration (DSA), which has been developed as a general term applied to describe the charged-particle acceleration process at shocks in which the particle distribution function is nearly isotropic (Giacalone et al. 1997). It assumes that all particles undergo a diffusive transport process by self-generated or pre-existing turbulence upstream and downstream of the shock so that they cross it back and forth many times. When particles interact with the shock, they may undergo first-order Fermi acceleration or/and drift acceleration (for non-parallel shocks), and eventually they experience a cumulative acceleration effect during multiple shock encounters. Conventionally, the DSA process is described by the diffusion–convection equation (Parker 1965; also called the Parker equation) that governs the evolution of the pitch-angle-averaged distribution function of energetic particles, with the basic assumption that the distribution function of particles is isotropic to first order ($O(u/v)$). It requires that particle velocities measured in the local plasma frame be far larger than the plasma flow speed in the shock frame (Zank et al. 2001).

However, the sources of the energetic particles in the heliosphere are usually regarded as low-energy thermal or suprathermal ions of solar and interplanetary origin (e.g., Zank et al. 2001; Mason et al. 2005, 2012; Desai et al. 2003, 2006; Desai & Burgess 2008). For example, there is strong evidence that a small portion of thermal and suprathermal particles from hot corona material or remnants of previous solar energetic particle (SEP) events serve as the source of large SEP events (Desai et al. 2006). Some models on SEP acceleration at coronal-mass-ejection-(CME)-driven shocks based on DSA theory show great promise in explaining SEP observations of specific gradual SEP events (e.g., Zank et al. 2000; Li et al. 2003, 2005; Tylka & Lee 2006; Verkhoglyadova et al. 2009, 2010, 2012). However, many DSA models assumed that the injection of the SEP source occurs at sufficiently high speeds $v \gg V_c = V_{\rm sh}/\cos\theta_{Bn}$, where v and $V_{\rm sh}$ are the particle speed and shock speed measured in the local plasma frame, respectively, θ_{Bn} is the shock obliquity, and V_c is the estimated injection threshold (Sandroos & Vainio 2007, 2009; Neergaard Parker & Zank 2012), so that particles can cross the shock back and forth in a diffusive manner. It is not clear what percentage of particles can be injected if their speed is lower than or close to the threshold. To build more powerful SEP models, it is necessary to model the detailed particle injection and acceleration process for source particles at lower energies close to the injection threshold, where the phase space density is usually higher than that at higher energies. At the termination shock, low-energy termination shock particles (TSPs) have been observed in the foreshock region with energy below ~20 MeV (Stone et al. 2005). The acceleration of pickup ions by the termination shock is believed to be responsible for the formation of TSPs. But the observations of spacecraft *Voyager 1* and *Voyager 2* indicate that TSPs are highly anisotropic in the foreshock region as a beam directly along the heliospheric magnetic field near the termination shock (Decker et al. 2005). Thus, traditional DSA theory is not adequate to describe the acceleration process of these particles. Besides, pickup ions have been observed to be efficiently injected into the acceleration process by the forward–reverse shock pair, the bound of corotating interaction regions (CIRs; Gloeckler et al. 1994; Scholer et al. 1999). In CIRs, pickup ions have speeds between zero and twice the solar wind speed, and thus part of the pickup ion distribution constitutes a suprathermal particle population. At these energies, a large fraction of the particles do not have the speed to be able to reflect back upstream with large energy gain, which leads to a large anisotropy.

In recent years, there have been some successful attempts to use the focused transport equation (FTE; Roelof 1969; Skilling 1975; Isenberg 1997), which was typically used to model the

propagation of SEPs produced by the CME-driven traveling shock in interplanetary space (e.g., Roelof 1969; Earl 1976; Bieber et al. 1980; Heras et al. 1992, 1995; Kallenrode 1993; Ruffolo 1995; Lario et al. 1998; Ng et al. 1999; Aran et al. 2007; Zhang et al. 2009; Qin et al. 2011; He et al. 2011; Wang et al. 2012) to model the shock acceleration process. For example, some researchers applied the FTE to investigate pickup ion acceleration by the termination shock (le Roux et al. 2007; le Roux & Webb 2009; Florinski et al. 2008a, 2008b; Zuo et al. 2011), and their simulations successfully reproduced nearly every essential observational feature of low-energy TSPs, such as a multiple power-law spectrum, the anisotropic distribution, and the intensity spike near the shock, all of which cannot be understood from standard DSA theory. Some recent studies on the physical process and modeling of SEP acceleration at CME-driven shocks were also implemented in the framework of focused transport theory (Kóta et al. 2005; Vainio & Laitinen 2007; Ng & Reames 2008; Battarbee et al. 2011; le Roux & Webb 2012) and considerable progress has been made. The FTE describes the evolution of the gyrotropic distribution function $f(\mathbf{x}, v, \mu)$ of energetic particles as space position $\mathbf{x}$, particle speed v, and pitch angle cosine $\mu = \cos\theta$. It treats the interaction of an energetic particle with magnetic irregularities as scattering and adiabatic focusing in the pitch angle. The applicability of the FTE to particle injection at shock waves is rooted in the fact that particles can only move upstream through large or small pitch angle scattering or focusing in combination with the speed of particle streaming. This is the fundamental difference with DSA theory, which relies on diffusion to send particles back upstream. Similar to the diffusion–convection equation, the FTE contains the principal physical mechanisms of particle acceleration, including first-order Fermi acceleration, drift acceleration, as well as second-order Fermi acceleration in the turbulent downstream (le Roux et al. 2007; Zuo et al. 2011). However, the equation is capable of solving the evolution of the particle in μ space with no restriction, allowing the particle distribution function to be highly anisotropic so that the near-isotropy limitation of DSA is lifted. It can treat the injection and acceleration of low-energy particles as well as the DSA process of high-energy particles in a unified way. In this sense, the focused transport theory is an extension of the standard DSA theory, thus it is a potential way to fill up the gap between knowledge of the source particles and the DSA process of high-energy particles.

In this study, we carry out a test particle simulation with a focused transport model to study the injection and acceleration of low-energy suprathermal particles at parallel shocks. Here, particles with low energies mean that the injection speed of source particles is below a few times the shock speed V_s (equal to the plasma speed in the shock frame), which corresponds to the energy of the most expected source particles (the solar wind particles presented in the suprathermal tail of the solar wind distribution or pickup ions). Our primary focus is on revealing the energy spectrum feature of the accelerated particles and the injection efficiency of the source, i.e., what are the portions of the injection source particles that can be accelerated to higher energies. In this simulation, we do not consider the shock dissipation during the acceleration process, assuming that the number of accelerated particles is too small to control the formation of shock. In addition, the effect of Alfvén waves generated by particles streaming away from the shock at the pitch angle scattering rate is not treated in a self-consistent manner. Instead, we use an assumed functional form of the pitch angle diffusion coefficients, which can be adjusted to take into account the overall level of turbulence expected at the shock. We will show that the shock strength, seed particle speed, and electric cross-shock potential (CSP) are basic factors that can affect the particle injection efficiency. Here, we do not treat the thermal particles with this test particle simulation. For thermal particles, the reformation of shock structure by the accelerated particles, nonlinear wave–particles, and wave–wave interactions needs to be taken into account, and the dissipation of kinetic energy into thermal energy at shocks is much more complicated. In Sections 2 and 3, we give the model details and the simulation results. A brief summary is presented in the last section.

2. FOCUSED TRANSPORT MODEL

The physical contents of the FTE for shock acceleration have been discussed in detail in le Roux & Webb (2009) and Zuo et al. (2011). For simplicity, we treat particle acceleration at planar shock under the assumption that the distribution function is only dependent on the spatial coordinate that is along the shock normal direction. With a single spatial dimension, the FTE is written as

$$\frac{\partial j_D}{\partial t} = -\left[\frac{\partial}{\partial x}(u + v\mu\cos\psi) + \frac{\partial}{\partial p}\left(\frac{dp}{dt}\right) + \frac{\partial}{\partial \mu}\left(\frac{\partial D_{\mu\mu}}{\partial \mu} + \frac{d\mu}{dt}\right)\right] j_D + \frac{\partial^2}{\partial \mu^2} D_{\mu\mu} j_D + Q(x, p, \mu) \quad (1)$$

$$\frac{dp}{dt} = -p\frac{du}{dx}\left(\frac{1-\mu^2}{2}\sin^2\psi + \mu^2\cos^2\psi + \frac{\mu u}{v}\cos\psi\right) + \mu q E_\parallel \quad (2)$$

$$\frac{d\mu}{dt} = \frac{1-\mu^2}{2}\frac{du}{dx}\left(\frac{v}{u}\sin^2\psi\cos\psi + \mu(1-3\cos^2\psi) - 2\frac{u}{v}\cos\psi\right) + \frac{(1-\mu^2)qE_\parallel}{p}, \quad (3)$$

where j_D is the particle differential number density, which is related to the pitch angle-averaged gyrotropic distribution function $f(x, \mu, p)$ by $j_D = 4\pi p^2 f$, and ψ is the angle between the magnetic field and the X-axis. Here, we define the X-axis, which denotes the unique spatial coordinates, along the shock normal from downstream to upstream, and the coplanar plane of the plasma flow and magnetic fields as the x–y plane. Note that the variables of the momentum p, pitch angle cosine μ, and the parallel electric $E_\parallel$ that arises from the cross-shock electric potential are defined in the local solar wind plasma frame, while the spatial coordinate x is defined in a fixed frame at the shock. $Q(x, p, \mu)$ is the source term of particle injection. In this simplified transport equation, the terms containing the stochastic acceleration that is not considered in this shock acceleration model are dropped. The momentum change dp/dt (Equation (2)) contains the adiabatic cooling or gain, acceleration by the parallel electric field in the plasma frame, and acceleration by inertia force in the plasma frame. The pitch angle change $d\mu/dt$ (Equation (3)) is not merely limited to small pitch angle scattering. It contains the focus on the non-uniform magnetic field and the pitch angle change due to both anisotropic adiabatic momentum loss and acceleration

by the parallel electric field and by inertia force. The plasma flow is normally incident ($\mathbf{U} = u\mathbf{e}_x$). We model the compressional flow in the thin ramp transition simply by using a linear profile. The magnetic field profile in the ramp can be computed using the continuity condition of the tangential electric field and conservation of magnetic flux ($u_x B_y = \text{Const}$, $B_x = \text{Const}$).

The FTE contains in its first-order derivative terms the results of the general guiding center kinetic transport theory, which conserves the particle's magnetic moment in both the plasma and de Hoffmann–Teller frames (le Roux & Webb 2009). The diffusion terms break the adiabatic invariant. In the above equations, we neglect the perpendicular diffusion since at a parallel shock it is much smaller relative to the parallel diffusion that arises from pitch angle scattering. For the pitch angle diffusion coefficient $D_{\mu\mu}$, we follow the form used in the work of le Roux et al. (2007) and le Roux & Webb (2009). We do not aim to get a complete self-consistent solution of the wave–particle interaction, but the level of scattering can be adjusted according to expected wave amplitude in the region near the shock. The expression $D_{\mu\mu}$ is given as (Schlickeiser 1989)

$$D_{\mu\mu} = D_0 \left[\left(\frac{1}{1+\epsilon} \right) \left(1 - \frac{\mu V_A}{v} \right) \frac{|v\mu - V_A|^{2/3}}{|v\mu - V_A|^{5/3} + (\Omega l_b)^{5/3}} \right] + D_0 \left[\left(\frac{\epsilon}{1+\epsilon} \right) \left(1 + \frac{\mu V_A}{v} \right) \frac{|v\mu + V_A|^{2/3}}{|v\mu + V_A|^{5/3} + (\Omega l_b)^{5/3}} \right] \quad (4)$$

with $D_0 = (\pi/8) A^2 \Omega^2 l_b (1-\mu^2)$. Here, the parameters V_A, ϵ, Ω, l_b, and A^2 are the Alfvén speed, the relative ratio of backward and forward propagating Alfvén waves, the gyrofrequency of particles, the correlation length, and the wave energy density of magnetic field fluctuation ($A^2 = (\delta B/B)^2$), respectively. For more details, please refer to le Roux et al. (2007) and le Roux & Webb (2009).

This transport equation is a three-dimensional parabolic differential equation (one spatial coordinate, momentum, and pitch angle). In our model, it is solved through a stochastic approach based on the mathematical equivalence between the Fokker–Planck diffusion problem and the system of stochastic differential equations (SDEs). It has been proved as a computationally efficient solution of the FTE and is able to avoid the numerical diffusion problems faced in some finite-difference solutions (Zhang et al. 2009; He & Qin 2011; Qin et al. 2011; Zuo et al. 2011). SDEs govern a class of stochastic pseudo particle trajectories. In previous applications, it was frequently integrated with a time-backward algorithm for a given boundary condition. However, for modeling particle injection from a given particle source, it may be more appropriate to perform the time-forward integration. The corresponding set of forward SDEs is as follows:

$$\begin{cases} dx = (u + v\mu\cos\psi)dt \\ dp = \frac{dp}{dt}dt \\ d\mu = \sqrt{2D_{\mu\mu}}d\omega(t) + \left(\frac{\partial D_{\mu\mu}}{\partial \mu} + \frac{d\mu}{dt} \right) dt \end{cases} . \quad (5)$$

Our stochastic simulation using the forward SDEs proceeds as follows to calculate the distribution function $f(x, p, \mu) = j_D(x, p, \mu)/4\pi p^2$: first, the particles are injected at $X = 0$ continuously from $t = 0$ to the time $t = t_{\max}$. Since the velocity distribution of the injected particles is considered to be isotropic in the plasma frame, the associated pitch angle cosine (μ) is selected as a random number from a uniform distribution in the range of $[-1,1]$. Then SDEs are solved to get the trajectory of each particle from the injection at $t = t_0$ to the ending time $t = t_{\max}$. The SDEs can be solved using the Runge–Kutta finite-difference algorithm, as we do for a set of first-order ordinary differential equations. The end status (x_e, p_e, μ_e) of each particle is recorded. Additionally, a free escape boundary is set in the upstream and downstream regions. If the particle reaches the free escape boundary, the calculation for the particle motion ends and the particle is thrown away. To minimize the escape of high-energy particles that could lead to a spectrum rollover, the free escape boundary is put in several diffusive lengths l_{diff} of the particles with a sufficiently high speed (equal to 100 times shock speed). Finally, the particle differential number density j_D can be statistically constructed by calculating the number density of particles in the phase space.

3. SIMULATION RESULTS

In this section, we discuss the fundamental properties of low-energy particle acceleration at parallel shocks. We consider a mono-energetic and isotropic source injection, i.e., the source term is given by $Q(x, p, \mu) = Q_0 \delta(p - p_0)\delta(x)$, where Q_0 is the particle injection rate. Here, we only consider cases with stable shock acceleration, i.e., the dynamic effect of suprathermal low-energy particles on shock formation is neglected. The spectrum of energetic particles downstream $f(p, p_0)$ from an upstream mono-energetic source can be regarded as a spectral transformation function. Given any true upstream ion spectrum $f_u(p_0)$, the post-shock ion spectrum can be easily calculated by integrating the pre-shock spectrum with the shock spectral transformation function appropriate for the shock condition, i.e., $f_d(p) = \int f_u(p_0) f(p, p_0) dp_0$.

For the DSA theory, the role of CSP is not taken into account since it is generally considered to have little effect on the acceleration of high-energy particles. To compare with the results from the DSA theory, we first neglect the CSP by setting its jump $\Delta\phi = 0$. Particle acceleration by shocks with different shock strength (compression ratio) is simulated. In the first cases, we set the particle injection speed v_0 equal to the shock speed in the plasma frame. Figure 1 shows the energy spectrum of the accelerated particles downstream of the shock (left) and the pitch angle distribution (PAD) of all the particles at all energies in the upstream region (right) for the cases of particle acceleration by weak (compression ratio $s = 1.75$), moderate ($s = 2.5$), and strong ($s = 3.0$) shocks, respectively. It can be seen that the upstream PADs are highly anisotropic, especially for the ions with pitch angle $\mu < 0$ that are transmitted from downstream. Here, we define a first-order anisotropy as

$$\xi = \frac{f(\mu)_{\max} - f(\mu)_{\min}}{f(\mu)_{\max} + f(\mu)_{\min}} \quad (6)$$

to describe the intensity of anisotropy. The first-order anisotropy is $\xi = 0.97$, 0.67, and 0.53 where $s = 1.75$, 2.5, and 3.0, respectively. This means that the anisotropy becomes much larger if the shock is weak. This is because there are more low-energy particles at a weak shock, which generally have stronger anisotropies. The shape of each energy spectrum is nearly consistent, which can be roughly divided into three parts: a complicated low-energy (compared to the shock ramp energy) spectrum, a spectrum rollover at high energies, and a power-law spectrum in between. It is consistent with the results of Zuo et al. (2011) and le Roux et al. (2007), both of which investigated the pickup ion acceleration spectrum at the termination shock.

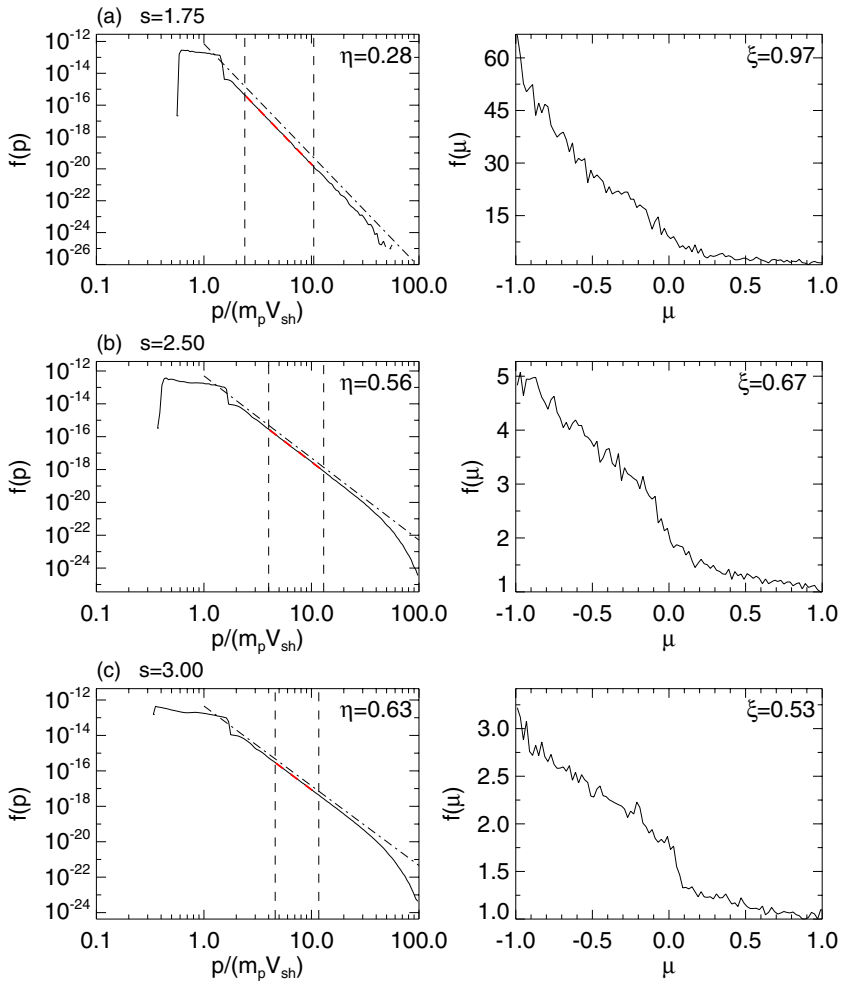

Figure 1. Energy spectrum of accelerated particles in the downstream of the shock and the pitch angle distribution of all the particles in the upstream region. The injection speed is given as equal to the shock speed in the plasma frame. Three cases with different shock compression ratios are simulated: (A) $s = 1.75$, (B) $s = 2.50$, and (C) $s = 3.0$. The dashed dot line is the solution of the DSA theory.

(A color version of this figure is available in the online journal.)

The spectrum rollover is not a real physical phenomenon in this simulation, either due to the finite simulation time or because of the free escape boundary in the simulation that can affect the statistics of particles with high enough energies.

At parallel shocks, the magnetic field direction is always along the shock normal through the shock layer, and the motional electric field is zero, so that in the shock frame one particle does not experience any momentum change when crossing the shock if we do not consider the cross-shock electric field. Thus, the parallel velocity $v_\parallel = u + v\mu$ is unchanged through the shock layer in the shock frame, i.e.,

$$u_1 + v_1\mu_1 = u_2 + v_2\mu_2, \tag{7}$$

where u_1 and u_2 are the plasma speed upstream and downstream of the shock, respectively, and v_1 and v_2 are the particle speeds in the local plasma frame. In addition, the perpendicular velocity in the plasma frame, equal to that in the shock frame, is also conserved, i.e.,

$$v_1\sqrt{1-\mu_1^2} = v_2\sqrt{1-\mu_2^2}. \tag{8}$$

According to Equations (7) and (8), when a particle is transmitted from upstream to downstream, its momentum change is determined by

$$\frac{p_2}{p_1} = \sqrt{\left(1+\frac{\Delta u}{v_1}\mu_1\right)^2 + \left(\frac{\Delta u}{v_1}\right)^2(1-\mu_1^2)}. \tag{9}$$

In the upstream, the particles with pitch angle $-(u_1/v_1) < \mu < 1$ are able to be transmitted, as the condition of $u_1 + v_1\mu > 0$ is satisfied. After the original injected particles with speed v_1 have been transmitted downstream, their momentum is in the range of $[\sqrt{1+(\Delta u/v_1)^2 - 2(\Delta u/v_1)(u_1/v_1)},\ 1+(\Delta u/v_1)]p_1$ according to Equation (9). For example, for the case with $s = 1.75$ and $v_1 = u_1$ (see Figure 1(A)), this momentum is between 0.54 p_1 and 1.2 p_1. The one-time-transmitted particles constitute a large part of the low-energy component of the spectrum in this momentum range. The lowest momentum of 0.54 p_1 is right at the low-energy cutoff of the energy spectrum. For the other cases, we can reach the same conclusions. In the analysis of le Roux et al. (2007), the rest of the low-energy component with spectrum decreases followed by a little bump is made up by those particles scattered by the downstream turbulence back to encounter the shock, and is then transmitted downstream again.

The standard DSA theory can naturally predict a power-law spectrum, and the power-law index merely depends on the compression ratio. For the mono-energetic and isotropic

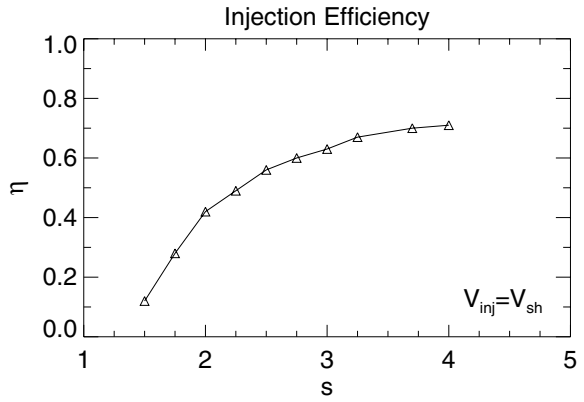

Figure 2. Injection efficiency as a function of the shock compression ratio (shock strength).

injection source $Q(x, p, \mu) = Q_0\delta(p - p_0)\delta(x)$, the analytical steady-state solution of the Parker equation for the downstream distribution function can be easily solved as $f(p) = (\gamma Q_0/4\pi u_1 p_0^3)p^{-\gamma}$ where γ is the spectral index with the expression $\gamma = 3s/(s - 1)$. The analytical solution is also presented in Figure 1 (see dashed dot lines). By comparison, it can be seen that the simulated power-law spectral index is always essentially the same as the prediction of DSA theory (see the fitting red lines), but the spectral intensity differs with different shock strengths. As pointed out by Zuo et al. (2011), the power-law spectrum is contributed by the particles that have multiple encounters with the shock. Here, we define the injection efficiency as the ratio of the intensity of the distribution function at the power-law energies obtained in the focused transport model to that given by the standard DSA theory, i.e., $\eta = f(p)/f_{\rm DSA}(p)$. It can be used to measure the relative acceleration rate, i.e., how many particles are accelerated into the diffusive acceleration regime. The injection efficiency is $\eta = 0.28$, 0.56, and 0.63 for the case with $s = 1.75$, 2.5, and 3.0, respectively. Figure 2 gives the injection efficiency variation along with the shock compression ratio (from $s = 1.5$ to $s = 4.0$, according to the results of a series of simulation cases). It can be seen that the injection efficiency is below 1 even for the strongest shock with $s = 4.0$. Some of these particles are decelerated ($p_2/p_1 < 0$) after one shock encounter and cannot return upstream for more acceleration. However, from the diffusion viewpoint, at least parts of these particles may return upstream, which is not applicable to the low-energy particles. The injection efficiency increases with the shock strength and indicates that the acceleration is more effective for a stronger shock. This is because stronger inertial force converts more kinetic energy into particle thermal energy.

Figure 3 shows how the energy spectrum and injection efficiency change with the injection speed for a given shock. Two series of cases are considered, one for a weak shock (given $s = 1.75$) and the other for a stronger shock ($s = 2.5$). The basic feature of the spectrum is that a power-law spectrum forms with a spectral index predicted by standard DSA theory similar to those shown in Figure 1. Figures 3(D) and (H) indicate that the injection efficiency increases abruptly with the injection speed. When the injection speed is high enough (for example, $v_{\rm inj} = 3.0\,V_{\rm sh}$; see Figures 3(C) and (G)), the injection efficiency approaches 1, which indicates that the spectral intensity already agrees with the standard DSA theory prediction. For shocks in the heliosphere (Earth's bow shock, CME-driven shocks or CIR-bounded shocks, and termination shock), the speed of suprathermal particles and the pickup ions (whether originally produced or accelerated by the heliospheric turbulence) is roughly a few times the shock speed. Our simulation indicates that there is no difficulty in injecting those particles into the DSA process for a parallel shock. For the injection particles with a fraction of shock speed, however, the effectiveness of the acceleration is poor.

The power-law spectrum is generally valid down to the particles with speed equal to a few times the upstream plasma speed. Figure 4 presents the PAD of the upstream particles at the energies corresponding to the power law. It is clear that these particles are still highly anisotropic. Bell (1978) and Drury (1983) pointed out that, from a microscopic viewpoint, the power-law spectrum is the natural consequence of the diffusive transport and multiple shock encounters of fast charged particles. In their derivations, the energy of particles is high enough when limited to either relativistic particles (Bell 1978) or superkinematic particles (Drury 1983), so that the scattering reaches a diffusive equilibrium and the particle anisotropy is small. For one particle with speed $v \gg \Delta u$ transmitted from upstream to downstream, the momentum change can be simplified from Equation (9) as

$$\frac{\Delta p}{p_1} = \frac{\Delta u}{v_1}\mu_1. \tag{10}$$

So for the transmitted particles with an isotropic distribution, the average momentum change is

$$\frac{\int_{-\frac{u}{v}}^{1} p\frac{\Delta u}{v}\mu^2 d\mu}{\int_{-\frac{u}{v}}^{1} \mu d\mu} \approx \frac{2}{3}\frac{\Delta u}{v}p. \tag{11}$$

In the same way, for the downstream particles with isotropy distribution re-crossing the shock in the upstream direction, the average momentum change is also $(2/3)(\Delta u/v)p$. Therefore, after one cycle, the ensemble average momentum change is $\delta p = (4/3)(\Delta u/v)p$. On the other hand, if the particles far downstream are isotropic, the escape probability by convection of a particle is $4u_2/v$. Combining the effects of two such factors, the rate of energy gain and the rate of loss by convection downstream, it can be derived that a power-law spectrum is expected to form and the spectrum index depends only on the shock compression ratio (Drury 1983). Note that from above derivation, this conclusion is correct merely under the following assumptions: (1) the particles in the far downstream are isotropic and (2) the particles that enter the shock ramp either in the upstream ($-(u_1/v) < \mu < 1$) or the downstream ($-1 < \mu < -(u_2/v)$) direction are isotropic or near isotropic. It is not necessary that the PAD in all directions is isotropic. In fact, from the right panel of Figure 4, we can see that PAD for the particles with $-1 < \mu < 0$ is highly anisotropic, but only the particles with $0 < \mu < 1$ may cross the shock from upstream, and these particles have a small anisotropy (see the red line). In addition, according to the simulation results with the focused transport model of le Roux et al. (2007), the PAD of particles in the downstream is uniform. The particles entering into the shock are nearly isotropic from both sides. It therefore explains why the power-law spectrum is still formed with the anisotropic treatment of the FTE in our simulation on the low-energy particle acceleration at parallel shocks.

Zank et al. (2001) proposed that at parallel and quasi-parallel shocks, particles incident on the shock can experience specular reflections either due to the CSP if the speed parallel with the shock normal is not high enough to overcome the potential

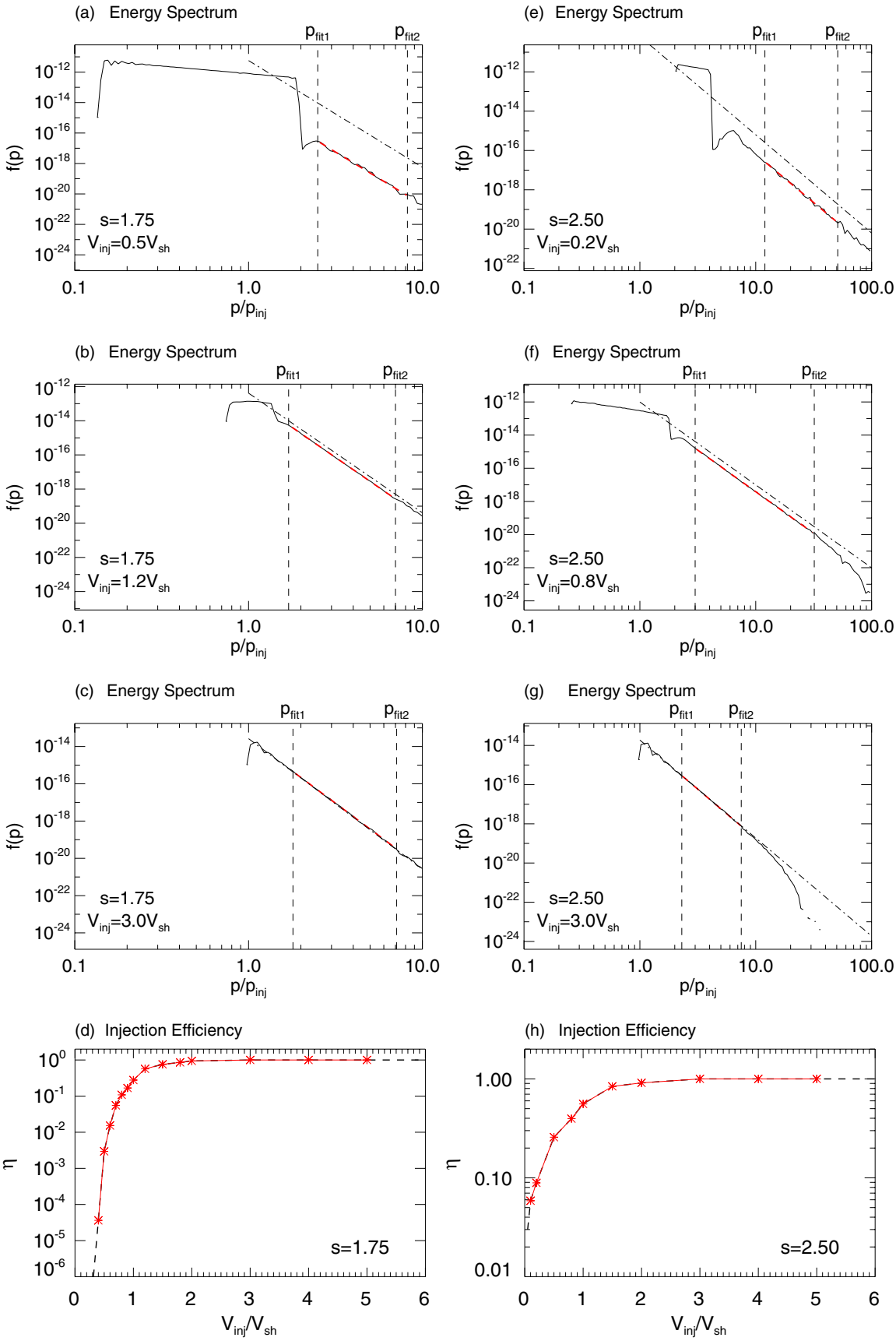

Figure 3. Selected energy spectra of the particles accelerated by parallel shocks from a mono-energy particle injection (A–C, E–G) and the injection efficiency variation with the injection speed (D and H). $p_{\rm fit1}$ and $p_{\rm fit2}$ denote the start and end point of the power-law spectrum, respectively. The dashed dot line is the solution of the diffusive shock acceleration theory.

(A color version of this figure is available in the online journal.)

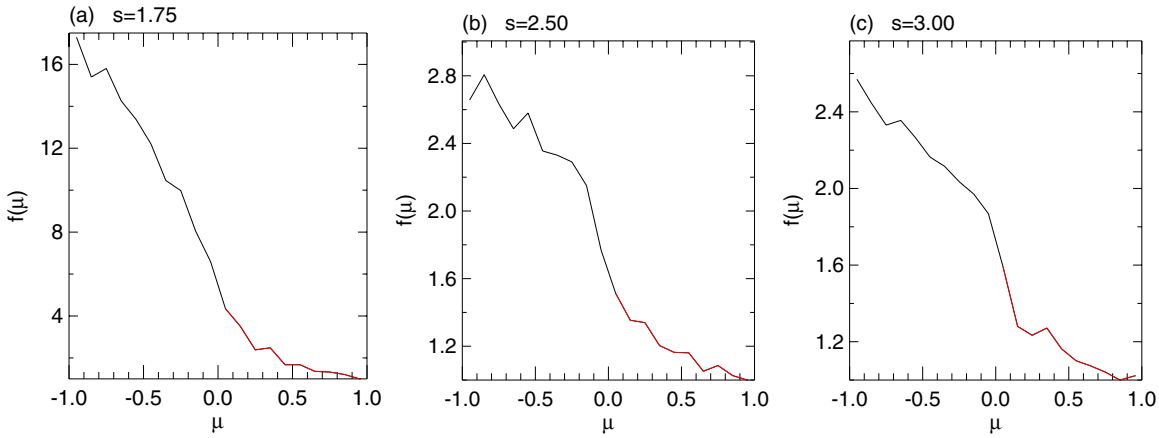

Figure 4. Pitch angle distribution of the particles in the upstream region with energies corresponding to the power-law distribution for the cases shown in Figure 1. (A color version of this figure is available in the online journal.)

barrier or as a result of the mirroring associated with the compressed magnetic field (only for oblique shocks). Each reflection boosts the energy of the ions viewed in the plasma frame. The reflected particles are trapped in the upstream by self-generated or pre-existing turbulence, which scatters the reflected particles and makes them return to the shock ramp and experience further acceleration. Eventually the turbulence and the CSP make a portion of particles, get multiple reflections, and gain sufficient energies. This energization process is called stochastic reflected ion (SRI) acceleration. Calculations on this mechanism have been done with an ideal magnetic shock geometry and a very thin shock ramp and it is found that SRI acceleration is very efficient for pickup ions that have a shell distribution (Zank et al. 2001). The CSP jump has a deceleration effect on the ions that transmit the shock from upstream, but also has an acceleration effect on the particles transmitted from downstream to upstream. In the FTE, particle reflection and energy gain or loss due to CSP are represented in the contribution of the parallel electric field to the momentum change and pitch angle change of energetic particles. The focused transport theory based on the FTE provides a unified framework to consider a different mechanism including SRI acceleration for parallel shocks. Hence, here we use the focused transport model to investigate the role of CSP in the injection and acceleration of low-energy particles at parallel shocks.

First, we re-investigate the pickup ion acceleration at parallel shocks when the CSP jump is taken into account. In the plasma frame, the speed of the pickup ions is taken to be equal to the upstream solar wind speed, and they have an isotropic shell distribution. The CSP jump is a frame-dependent parameter that is usually the function of the energy change of upstream plasma flow across the shock, i.e., $q\Delta\phi = \zeta((1/2)m_p u_1^2 - (1/2)m_p u_2^2)$. Currently, there is no definitive knowledge of the value of CSP. Cluster observations show that the CSP jump at Earth's bow shock is comparable to the ion kinetic energy change across the shock (Bale et al. 2008). The CSP is measured in the normal incident frame to be from a portion of to more than two times of the ion energy change with large variations (Bale et al. 2008). In the de Hoffmman–Teller frame or in the plasma frame, this value may be reduced because of a potential off-plane magnetic field in the shock ramp. Here, cases with a different ζ value given in the plasma frame, from very small to $\zeta = 1.0$, are simulated. Four representative plots with $\zeta = 0.1, 0.5, 0.8$, and 1.0, respectively, are presented in Figure 5 to show how the energy spectrum evolves. The compression ratio is $s = 2.5$. It can be seen that compared with Figure 1(B) where the CSP is not considered, the shape of the energy spectrum is basically unchanged. At high enough energies, there is still a power-law distribution with a spectral index the same as that given by the standard DSA theory. However, with the increasing CSP jump, the low-energy cutoff becomes higher, and the injection efficiency also increases (injection efficiency index η is 0.98, 2.30, 3.25, and 4.00 for ζ equal to 0.1, 0.5, 0.8, and 1.0 respectively). Low-energy cutoff is the lowest energy of the one-time-transmitted pickup ions. With no CSP, all the pickup ions upstream that interact with the shock layer for the first time are transmitted downstream. In the presence of the CSP jump, some particles are reflected if the speed parallel with the shock normal (the direction of magnetic field) is too low to overcome the CSP barrier, so that the energy range of the transmitted particles is changed to a higher cutoff. The injection efficiency increases when there is a larger CSP jump, consistent with the results of Zank et al. (2001). At parallel shocks, the specular reflection is only due to the CSP. For a stronger CSP jump, evidently more particles get a specular reflection since the lowest energy required for particles to overcome the potential barrier is raised. Thus, the reflection efficiency depends on the intensity of the CSP jump. This is the reason why the injection efficiency is larger for stronger CSP added in the simulations.

For high-energy particles, CSP becomes less important to their motion since the electric field force is relatively smaller than the Lorentz force. It also can be understood from the FTE. For parallel shocks (the magnetic field is not changed so that it is along with the shock normal with ψ always equal to zero), the momentum change rate and the pitch angle change rate, respectively, have the forms (see Equations (2) and (3))

$$\frac{1}{p}\frac{dp}{dt} = -\frac{du}{dx}\left(\mu^2 + \frac{\mu u}{v}\right) + \frac{\mu q E_\parallel}{p} \tag{12}$$

$$\frac{d\mu}{dt} = -(1-\mu^2)\frac{du}{dx}\left(\mu + \frac{u}{v}\right) + \frac{(1-\mu^2)qE_\parallel}{p}. \tag{13}$$

The corresponding contribution of the parallel electric field $E_\parallel$ (see the last term in each equation) is inversely proportional to the particle momentum. So if the particle's momentum is high enough, its role becomes very weak. Thus in DSA theory, the effect of CSP is usually neglected. Figure 6 shows the energy spectra for three cases with the injection speed v_0 being equal to 1.0, 3.0, and 8.0 times the shock speed, respectively. The black

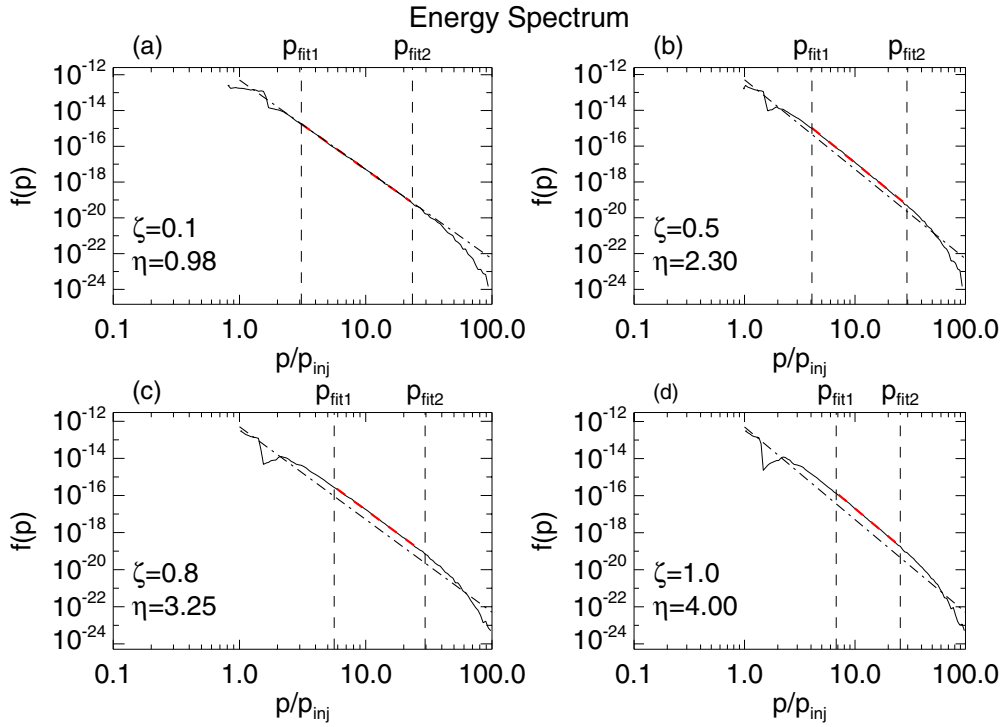

Figure 5. Energy spectrum of accelerated pickup ions by parallel shocks. The shocks have a cross-shock potential jump with various ζ values. The dashed dot line is the solution of the diffusive shock acceleration theory.

(A color version of this figure is available in the online journal.)

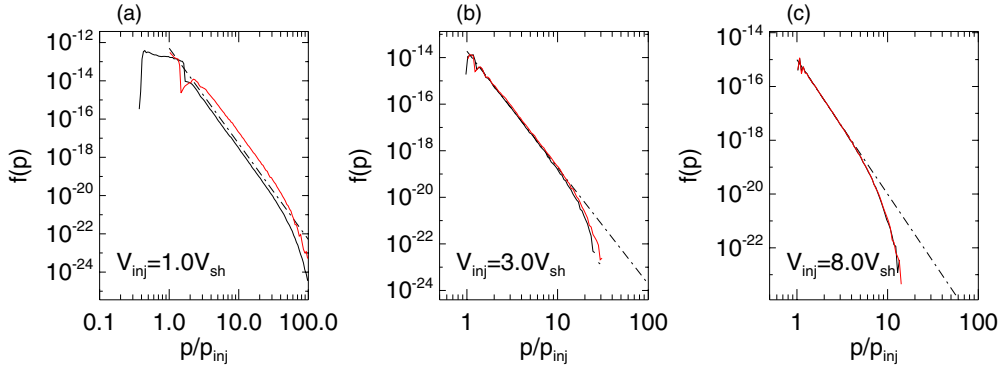

Figure 6. Comparison of energy spectra with (red solid line) and without (black solid line) a CSP jump. The injection speed of source particles is 1.0, 3.0, and 8.0 times shock speed in panels (A)–(C), respectively. The dashed dot line is the solution of the DSA theory.

(A color version of this figure is available in the online journal.)

lines are the spectra with no CSP jump considered and the red lines are those with CSP taken as $\zeta = 1.0$ (to show maximum possible effect, the high CSP value is chosen). Spectrum comparison shows that the CSP does not affect the slope of the power law at higher energies. For the case with $V_{\rm inj} = 1.0\ v_{sh}$, the injection efficiency is evidently enhanced (from $\eta = 0.57$ to $\eta = 4.0$) when the CSP is added (see Figure 6(A)). But if the injection speed of the source particles increases to, for example, $V_{\rm inj} = 3.0\ V_{\rm sh}$, the injection efficiency is almost unchanged (from $\eta = 1.0$ to $\eta = 1.05$; see Figure 6(B)). Figure 6(C) is presented for the case with $V_{\rm inj} = 8.0\ V_{\rm sh}$, a high-energy injection, and indicates that the spectra with and without CSP are essentially identical (apart from the rollover that is caused by the finite simulation domain or free escape boundary setting) and injection efficiency is kept at unity. This means that if the injection speed of source particle is high enough, the CSP basically has no effect on the acceleration process, and the DSA theory is completely applicable.

4. SUMMARY

Here, we present the energy spectra of low-energy ions accelerated by parallel shocks with a focused transport model. The acceleration process at shocks and particle transport in the upstream and downstream turbulent environments can be described in a unified way by the FTE. The FTE retains the pitch angle information so as to avoid the limitation of small pitch angle anisotropy inherent in DSA theory, thus making the focused transport theory an extension of DSA theory. The focused transport model enables us to investigate how the low-energy suprathermal particles are directly injected and accelerated by shocks, even though they are usually anisotropic in the acceleration process. Some models with hybrid simulations (e.g., Liewer et al. 1993, 1995; Kucharek & Scholer 1995; Giacalone & Ellison 2000; Scholer et al. 2002; Giacalone 2003, 2005; Su et al. 2012) also have the ability to study the dynamic of thermal or suprathermal particles at shocks. By comparison,

the focused transport model through solving the macroscopic diffusion problem with parameterized treatment is relatively uncomplicated and can easily be used to model the dynamic of particles on very large scales, such as the SEP acceleration and propagation in the global heliospheric magnetic field.

From this test particle simulation, we found that the particles with the speed of a fraction of to a few times the shock speed can indeed be directly injected and accelerated by parallel shocks. The low-energy suprathermal particles interact with the upstream and downstream turbulence media and the shock in the same way as the accelerated high-energy populations. The accelerated energy spectrum consists of two components: a low-energy component, which is made up by the particles interacting with the shock once or a few times, and a power-law high-energy component contributed by particles with multiple shock encounters starting from a few times the shock speed. The spectral index is the same as the solution of standard DSA theory, although the particles have a large anisotropy in the upstream region, but the injection efficiency is much different. These are basic features of the low-energy particle acceleration at parallel shocks. The shock strength, injection speed of the source particles, and CSP are three major factors that affect the injection efficiency. Consistent with our conventional knowledge, the injection efficiency is larger for stronger shocks. We also study the injection efficiency at a given shock for different injection speeds of particles. It is found that the injection efficiency rapidly increases with the injection speed. The CSP jump, although it is not easy to determine its value by observations, also can affect the acceleration process. The injection efficiency is higher if there is a larger CSP jump. Here, we also verify that CSP has very little effect on the acceleration of particles with high enough energy. Moreover, if the injection speed is above a few times the shock speed, both the intensity and the index of the power-law spectrum are consistent with the prediction of standard DSA theory, i.e., DSA theory and the focused transport model arrive at nearly the same solution. It can be concluded that the focused transport theory is essentially an extension of DSA theory.

This work was supported in part by NASA under Grants NNX08AP91G, NNX09AG29G, and NNX09AB24G, NSF grant AGS-1156056, and NSF under MRI Grant 0923050. We thank Marcus Hohlmann and his High Energy Physics group at Florida Tech for making their high-performance grid computing cluster available for some of the computational analysis presented here.

REFERENCES

Aran, A., Lario, D., Sanahuja, B., et al. 2007, A&A, 469, 1123
Bale, S. D., Mozer, F. S., & Krasnoselskikh, V. V. 2008, arXiv:0809.2435
Battarbee, M., Laitinen, T., & Vainio, R. 2011, A&A, 535, A34
Bell, A. R. 1978, MNRAS, 182, 147
Bieber, J. W., Earl, J. A., Green, G., et al. 1980, JGR, 85, 2313
Decker, R. B., Krimigis, S. M., Roelof, E. C., et al. 2005, Sci, 309, 2020
Desai, M. I., & Burgess, D. 2008, JGR, 113, A00B06
Desai, M. I., Mason, G. M., Dwyer, J. R., et al. 2003, ApJ, 588, 1149
Desai, M. I., Mason, G. M., Mazur, J. E., & Dwyer, J. R. 2006, SSRv, 124, 261
Drury, L. Oc. 1983, RPPh, 46, 973
Earl, J. A. 1976, ApJ, 205, 900
Florinski, V., Decker, R. B., & le Roux, J. A. 2008a, JGR, 113, A07103
Florinski, V., Zank, G. P., & le Roux, J. A. 2008b, AdSpR, 41, 361
Giacalone, J. 2003, P&SS, 51, 659
Giacalone, J. 2005, ApJL, 628, L37
Giacalone, J., Burgess, D., Schwartz, S. J., Ellison, D. C., & Bennett, L. 1997, JGR, 102, 19789
Giacalone, J., & Ellison, D. C. 2000, JGR, 105, 12541
Gloeckler, G., Geiss, J., Roelof, E. C., et al. 1994, JGR, 99, 17637
He, H. Q., & Qin, G. 2011, ApJ, 730, 46
He, H. Q., Qin, G., & Zhang, M. 2011, ApJ, 734, 74
Heras, A. M., Sanahuja, B., Lario, D., et al. 1995, ApJ, 445, 497
Heras, A. M., Sanahuja, B., Smith, Z. K., et al. 1992, ApJ, 391, 359
Isenberg, P. A. 1997, JGR, 102, 4719
Kallenrode, M. B. 1993, JGR, 98, 19037
Kóta, J., Manchester, W. B., Jokipii, J. R., de Zeeuw, D. L., & Gombosi, T. I. 2005, in AIP Conf. Proc., Vol. 781, The Physics of Collisionless Shocks, ed. G. Li, G. P. Zank, & C. T. Russell (Melville, NY: AIP), 201
Kucharek, H., & Scholer, M. 1995, JGR, 100, 1745
Lario, D., Sanahuja, B., & Heras, A. M. 1998, ApJ, 509, 415
le Roux, J. A., & Webb, G. M. 2009, ApJ, 693, 534
le Roux, J. A., & Webb, G. M. 2012, ApJ, 746, 104
le Roux, J. A., Webb, G. M., Florinski, V., & Zank, G. P. 2007, ApJ, 662, 350
Li, G., Zank, G. P., & Rice, W. K. M. 2003, JGR, 108, 1082
Li, G., Zank, G. P., & Rice, W. K. M. 2005, JGR, 110, A06104
Liewer, P. C., Goldstein, B. E., & Omidi, N. 1993, JGR, 98, 15,211
Liewer, P. C., Rath, S., & Goldstein, B. E. 1995, JGR, 100, 19,809
Mason, G. M., Desai, M. I., & Li, G. 2012, ApJL, 748, L31
Mason, G. M., Desai, M. I., Mazur, J. E., & Dwyer, J. R. 2005, in AIP Conf. Proc. 781, The Physics of Collisionless Shocks, ed. G. Li, G. P. Zank, & C. T. Russell (Melville, NY: AIP), 219
Neergaard Parker, L., & Zank, G. P. 2012, ApJ, 757, 97
Ng, C. K., & Reames, D. V. 2008, ApJL, 686, L123
Ng, C. K., Reames, D. V., & Tylka, A. J. 1999, GeoRL, 26, 2145
Parker, E. N. 1965, P&SS, 13, 9
Qin, G., He, H. Q., & Zhang, M. 2011, ApJ, 738, 28
Roelof, E. C. 1969, in Lectures in High-energy Astrophysics, ed. H. Ogelmann & J. R. Wayland (SP-199; Washington, DC: GPO), 111
Ruffolo, D. 1995, ApJ, 442, 861
Sandroos, A., & Vainio, R. 2007, ApJL, 662, L127
Sandroos, A., & Vainio, R. 2009, ApJS, 181, 183
Schlickeiser, R. 1989, ApJ, 336, 243
Scholer, M., Kucharek, H., & Kato, C. 2002, PhPl, 9, 4293
Scholer, M., Mann, G., Chalov, S., et al. 1999, SSRv, 89, 369
Skilling, J. 1975, MNRAS, 172, 557
Stone, E. C., Cummings, A. C., McDonald, F. B., et al. 2005, Sci, 309, 2017
Su, Y. Q., Lu, Q. M., Huang, C., et al. 2012, JGR, 117, A08107
Tylka, A. J., & Lee, M. A. 2006, ApJ, 646, 1319
Vainio, R., & Laitinen, T. 2007, ApJ, 658, 622
Verkhoglyadova, O. P., Li, G., Ao, X., & Zank, G. P. 2012, ApJ, 757, 75
Verkhoglyadova, O. P., Li, G., Zank, G. P., et al. 2010, JGR, 115, A12103
Verkhoglyadova, O. P., Li, G., Zank, G. P., Hu, Q., & Mewaldt, R. A. 2009, ApJ, 693, 894
Wang, Y., Qin, G., & Zhang, M. 2012, ApJ, 752, 37
Zank, G. P., Rice, W. K. M., Le Roux, J. A., Cairns, I. H., & Webb, G. M. 2001, PhPl, 8, 4560
Zank, G. P., Rice, W. K. M., & Wu, C. C. 2000, JGR, 105, 25079
Zhang, M., Qin, G., & Rassoul, H. 2009, ApJ, 692, 109
Zuo, P. B., Zhang, M., Gamayunov, K., Rassoul, H., & Luo, X. 2011, ApJ, 738, 168